iScience

CellPress
OPEN ACCESS

Article

Chromosomes distribute randomly to, but not within, human neutrophil nuclear lobes

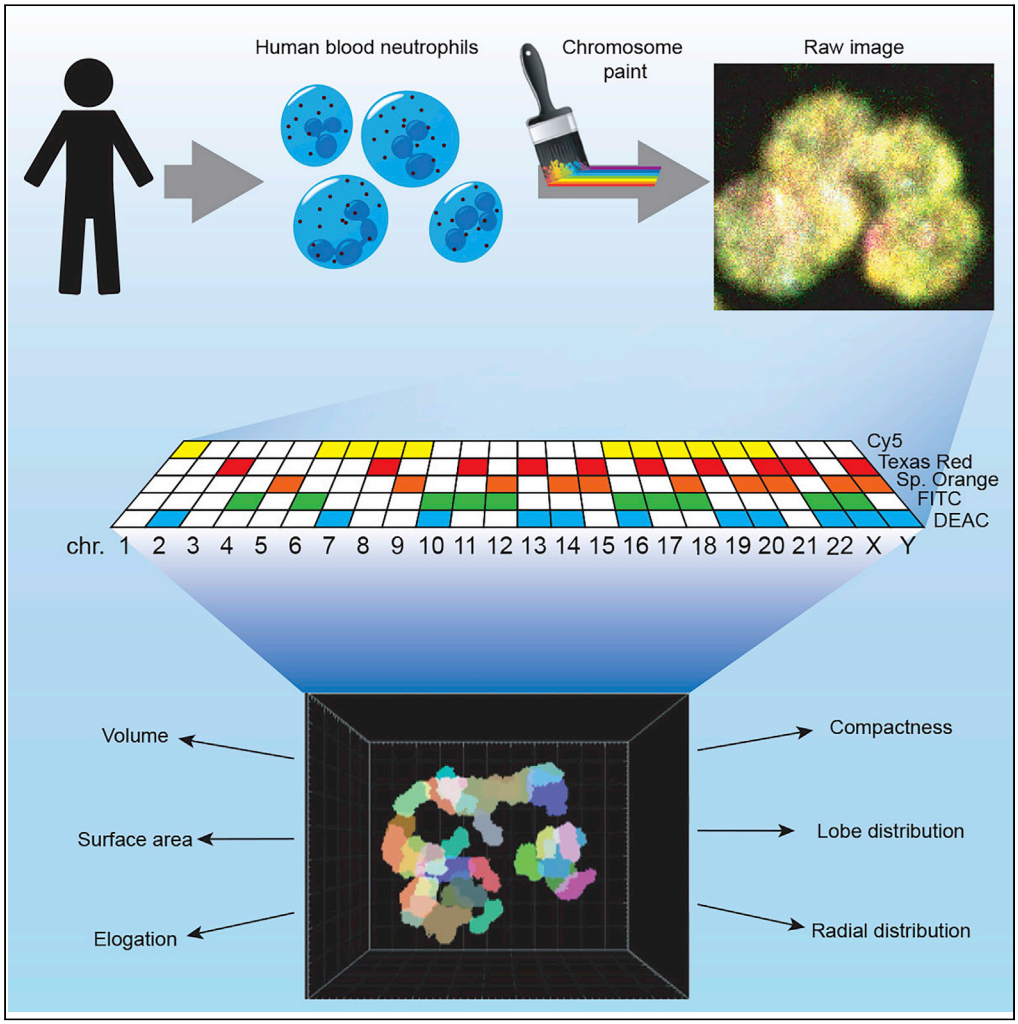

Christine R. Keenan, Michael J. Mlodzianoski, Hannah D. Coughlan, ..., Thomas Boudier, Rhys S. Allan, Timothy M. Johanson

johanson@wehi.edu.au

HIGHLIGHTS

Human chromosomes randomly distribute to neutrophil nuclear lobes

However, they sustain a non-random radial distribution within these lobes

Chromosome length correlates with volume in neutrophils and other human immune cells

Gene-regulatory transchromosomal interactions are unlikely in human neutrophils

Keenan et al., iScience 24, 102161
March 19, 2021
https://doi.org/10.1016/j.isci.2021.102161

iScience

CellPress
OPEN ACCESS

Article

Chromosomes distribute randomly to, but not within, human neutrophil nuclear lobes

Christine R. Keenan,[1,2,5] Michael J. Mlodzianoski,[1,2,5] Hannah D. Coughlan,[1,2] Naiara G. Bediaga,[1,2] Gaetano Naselli,[1,2] Erin C. Lucas,[1,2] Qike Wang,[1,2] Carolyn A. de Graaf,[1,2] Douglas J. Hilton,[1,2] Leonard C. Harrison,[1,2] Gordon K. Smyth,[1,3] Kelly L. Rogers,[1,2] Thomas Boudier,[1,2,4] Rhys S. Allan,[1,2,6] and Timothy M. Johanson[1,2,6,7,*]

SUMMARY

The proximity pattern and radial distribution of chromosome territories within spherical nuclei are random and non-random, respectively. Whether this distribution pattern is conserved in the partitioned or lobed nuclei of polymorphonuclear cells is unclear. Here we use chromosome paint technology to examine the chromosome territories of all 46 chromosomes in hundreds of single human neutrophils – an abundant and famously polymorphonuclear immune cell. By comparing the distribution of chromosomes to randomly shuffled controls and validating with orthogonal chromosome conformation capture technology, we show for the first time that human chromosomes randomly distribute to neutrophil nuclear lobes, while maintaining a non-random radial distribution within these lobes. Furthermore, we demonstrate that chromosome length correlates with three-dimensional volume not only in neutrophils but other human immune cells. This work demonstrates that chromosomes are largely passive passengers during the neutrophil lobing process but are able to subsequently maintain their macro-level organization within lobes.

INTRODUCTION

First proposed in 1885 (Rabl, 1885) and with vacillating levels of acceptance until recent decades, interphase chromosomes maintaining a territorial organization is now a widely accepted principle of nuclear organization in most eukaryotes (Cremer and Cremer, 2010). This is unsurprising, given the importance of this organization to functions as fundamental as gene expression and DNA repair. For example, the radial position of a chromosome within the nucleus is strongly correlated with its transcriptional activity and gene density (Cremer and Cremer, 2010). Furthermore, the proximity of chromosomes to one another (both homologous and non-homologous) is thought to be important during DNA repair (Agmon et al., 2013) and potentially even in direct gene regulation (Hewitt et al., 2008; Kim et al., 2014; Ling et al., 2006; Spilianakis et al., 2005; Zhao et al., 2006).

While the radial distribution of chromosomes is well understood to be non-random (Cremer and Cremer, 2010), the position of chromosomes relative to each other, or proximity pattern, is contentious, with reports of both non-random (Brianna Caddle et al., 2007; Parada et al., 2002, 2004; Roix et al., 2003; Khalil et al., 2007) and random distributions (Bolzer et al., 2005). In the absence of being able to observe interphase chromosome movements in live cells over long periods of time, combined with the absence of physical barriers to restrict chromosome movement, it is possible that these studies simply differ in their detection of transient or infrequent interphase chromosomal interactions or movements.

Human neutrophils constitute approximately two-thirds of the immune cells in human blood. They are readily identifiable by their polymorphonuclear nature with their nuclei being segmented into 2–6 lobes joined only by thin filaments of nucleoplasm (P Ehrlich, 1900). Here we exploit this natural nuclear segmentation to examine the importance of interphase chromosome distribution. We hypothesize that if

[1]The Walter and Eliza Hall Institute of Medical Research, Parkville, VIC, 3052, Australia

[2]Department of Medical Biology, The University of Melbourne, Parkville, VIC, 3010, Australia

[3]School of Mathematics and Statistics, The University of Melbourne, Parkville, VIC, 3010, Australia

[4]Institute of Biology Paris-Seine, Sorbonne Université, Paris, France

[5]These authors contributed equally

[6]These authors contributed equally

[7]Lead contact

*Correspondence: johanson@wehi.edu.au

https://doi.org/10.1016/j.isci.2021.102161

interactions between chromosomes are biologically important these chromosomes would preferentially locate together into neutrophil nuclear lobes, enabling continuing interaction.

Using chromosome paint technology alongside high-throughput image analysis pipelines, we have examined all 46 human chromosomes in 240 single neutrophil nuclei. We reveal that while the radial distribution of chromosomes within neutrophil nuclear lobes is non-random, the distribution of chromosomes to lobes is random.

RESULTS

Analysis pipeline detects the position and characteristics of all human chromosomes in three-dimensions.

Given the complexity of examining all 46 human chromosomes in hundreds of single, segmented neutrophil nuclei, we developed a bespoke image analysis pipeline to detect the position and three-dimensional characteristics of all chromosomes in images generated using chromosome paint.

In brief, each of the 22 autosome pairs and the X and Y chromosomes within fixed healthy male human blood neutrophil nuclei (Figure S1A) is "painted" with a specific combination of fluorescent probes within the chromosome paint mix (Figures 1A and 1B and Supplemental information). The whole nucleus is then imaged and analyzed using our analysis pipeline (Figure 1C). First, the intensity of each of the five channels in each individual image is normalized. A malleable grid with lines that flex to incorporate nearby voxels of similar channel intensity patterns is then applied to each image. This flexibility allows the grid to capture the highly variable three-dimensional shapes formed by chromosomes. Adjacent cubes of the grid that share channel intensities are then combined to create "objects". Based upon the expected spectral combinations for each chromosome (Figure 1B), these objects are then assigned as chromosomes (Figure S1B and Videos S1, S2, and S3). This analysis pipeline was initially validated using human metaphase chromosome spreads where it reliably called whole, individual chromosomes (e.g. >95% of objects were called with a single chromosome identity) (Figure S1C). To avoid the common pitfall of arbitrary thresholding to define genuine signal from background (Cremer and Cremer, 2010), every image was assigned an individually determined threshold. This threshold is calculated by automated sequential testing of various thresholds to determine the value which maximizes the number of objects with genuine chromosome channel combinations, while minimizing spectrally spurious objects (e.g. detected objects that have a channel combination differing from the 24 specific chromosome combinations) (Figure S2).

Importantly, chromosome paint and our image analysis pipeline detects the majority of the 22 human autosomes and the sex chromosomes at approximately the expected proportions (Figures 1D and S3A). While some chromosomes appear more difficult to define or detect (e.g. chromosome 13, 15, 21, and 22), the proportions of chromosomes detected are similar across human immune cell types ($CD4^+$ and $CD8^+$ T cells) (Figures S3B and S3C), suggesting that the variation in detection frequency observed is technical, not biological.

We next examine the three-dimensional character of all 46 chromosomes, including volume (Figure 1E) and surface area (Figure 1F), among others (Figures S3D and S3E). While the physical characteristics of the chromosome territories varies greatly across neutrophil nuclei, the volume and surface area of the Y chromosomes are, as expected, consistently and significantly ($P = 0.02$ and $P = 0.04$, respectively) smaller than the X chromosome (Figures 1E and 1F).

While the differences in the three-dimensional character of the chromosomes are subtle, the ability to examine all chromosomes (as opposed to between 2 and 7 chromosomes (Aquiles Sanchez et al., 1997; Hubner et al., 2015; Yerle-Bouissou et al., 2009)) in large numbers of cells affords power. For example, previous studies suggest minimal relationship between chromosome linear length and three-dimensional volume (Aquiles Sanchez et al., 1997; Yerle-Bouissou et al., 2009), however, our analysis suggests a significant linear relationship between the two ($r^2 = 0.359$, $p = 0.001$), not only in neutrophils (Figure 1G) but also in other human immune cells (Figures S3F and S3G).

Thus, despite chromosome paint data containing variance in both chromosome detection and three-dimensional parameters, and the fact that fixation partly alters the morphology of nuclei (Hepperger

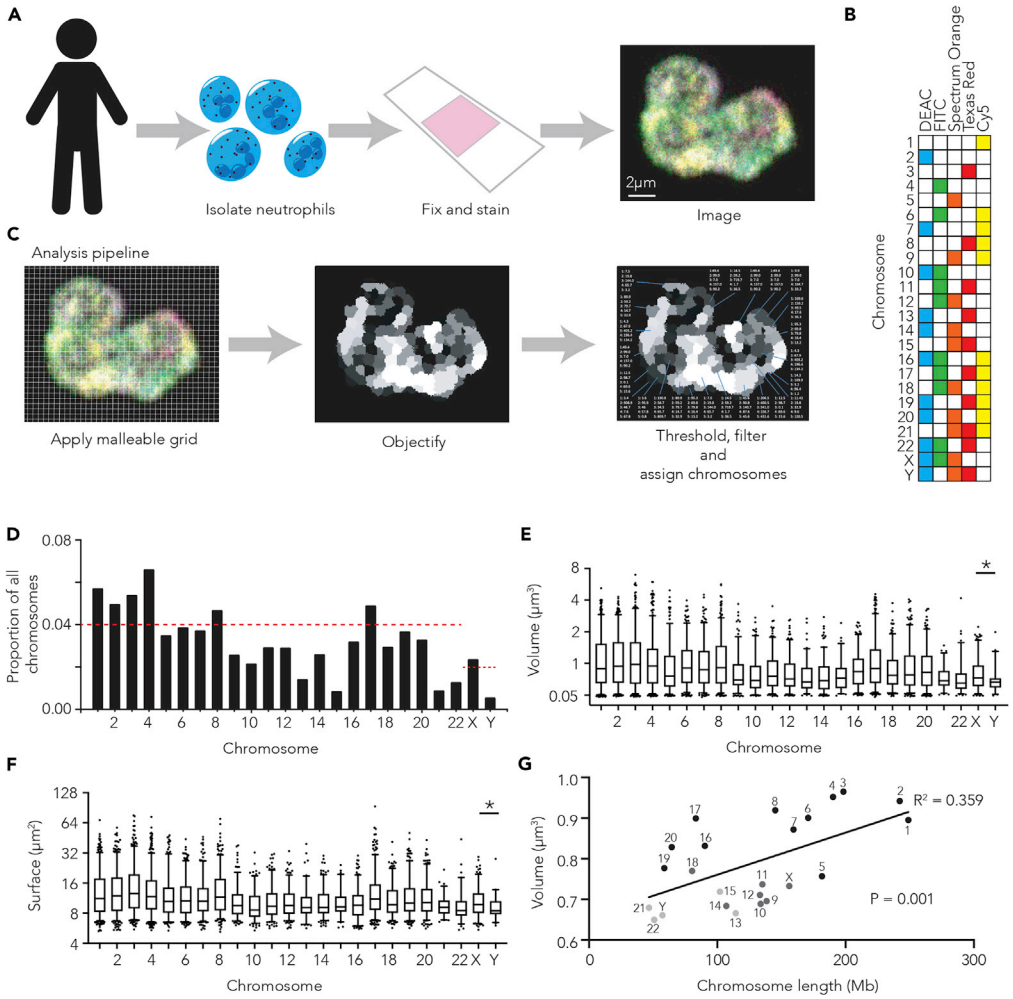

Figure 1. Analysis pipeline detects the position and characteristics of all human chromosomes in three-dimensions

(A–C) Schematic of neutrophil isolation, chromosome paint (A), spectral character of each human chromosome (B), and image analysis pipeline (C). (D) Proportion of total chromosomes detected made up by each chromosome in human blood neutrophils. Red line represents expected proportion if all 24 chromosomes were detected equally (0.04 for autosomes, 0.02 for sex chromosomes).

(E and F) Box and whisker plot (fifth-95th percentile) of the volume (μm^3) (E) and surface area (μm^2) (F) of each chromosome across all 240 neutrophils. Unpaired T test used to compare X and Y chromosomes.

(G) Plot of median chromosome volume across all neutrophils against chromosome linear length with straight line fitted ($y = 1.09e\text{-}3x+0.649$, $R^2 = 0.359$ and $P = 0.001$). Dark and light gray points indicate chromosome was called as less than 0.03 or 0.02 of all chromosomes respectively, as in Figure 1D.

et al., 2007), the scale of our data set allows elucidation of biologically important correlations and phenomena.

Human neutrophil chromosomes distribute randomly to nuclear lobes

There is conflicting evidence as to whether the proximity pattern of chromosomes is random or non-random, even within polymorphonuclear nuclei (Yerle-Bouissou et al., 2009; Hepperger et al., 2009; Karni et al., 2001; Aquiles Sanchez et al., 1997; Bartova et al., 2001).

In order to examine the distribution of chromosomes to neutrophil nuclear lobes, we first developed a high throughput pipeline to define the lobes. In brief, the pipeline uses watershed analysis from manually assigned seeds within each lobe (Figure S4A) to rapidly define nuclear lobes (Figure S4B). Consistent with

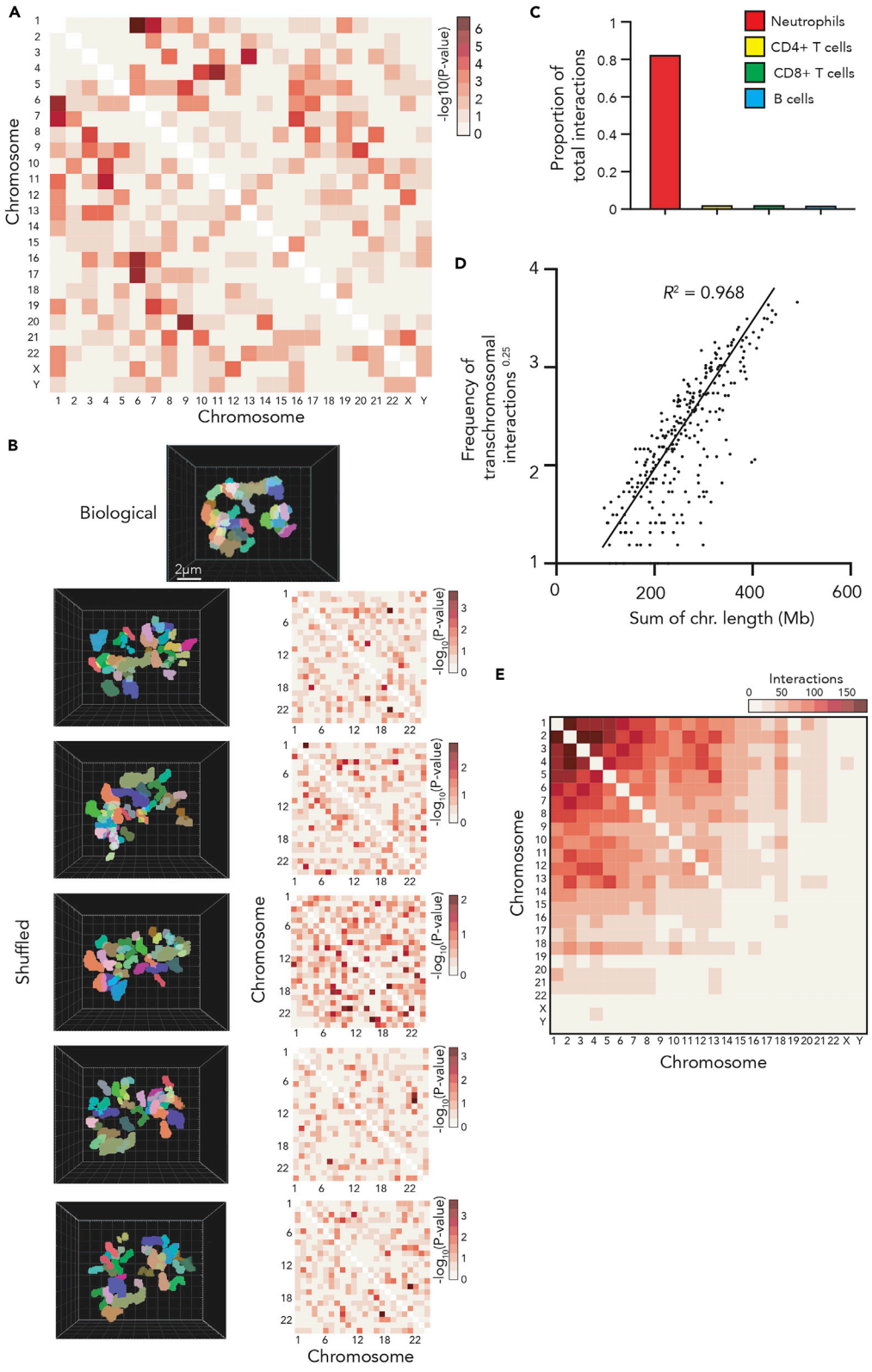
A
Chromosome
Chromosome
-log10(P-value)
B
Biological
2μm
Shuffled
Chromosome
-log10(P-value)
C
Proportion of total interactions
Neutrophils
CD4+ T cells
CD8+ T cells
B cells
D
Frequency of transchromosomal interactions 0.25
R² = 0.968
Sum of chr. length (Mb)
E
Interactions
Chromosome
Chromosome

Figure 2. Human neutrophil chromosomes distribute randomly to nuclear lobes

(A and B) (A) Heatmap of the -$\log_{10}$(p value) from chromosome lobe colocalization analysis in human blood neutrophil nuclear lobes. The analysis determined if pairs of chromosomes are found colocalized within a lobe at a higher rate than expected by chance (B) Top: Three-dimensional render of chromosomes within a human neutrophil nucleus. Left: Three-dimensional renders of the same neutrophil and chromosomes after five sets of random chromosome shuffling. Right: Heatmap of the -$\log_{10}$(p value) from the chromosome colocalization analysis of five independent sets of random chromosome shuffling.

(C and D) (C) Schematic of the proximity ligation reaction central to the *in situ* HiC protocol, (D) Proportion of total DNA-DNA interactions detected by *in situ* HiC and the *diffHiC* pipeline that occur between chromosomes (transchromosomal interactions) in human immune cells.

(E) Frequency of transchromosomal interactions to the power of 0.25, plotted as a function of summed chromosome length in human neutrophils. Straight line fitted to data with no intercept (y = 8.621e-3x, R^2 = 0.9683 and p value <2.2 × 10^{-16}).

(F) Heatmap of the number of transchromosomal interactions by each chromosome to all others in human neutrophils.

previous studies (Karni et al., 2001), we find that the majority of healthy human blood neutrophils have between 3 and 4 lobes (Figure S4C) of approximately equal volumes (Figure S4D).

Next, we performed a lobe colocalization analysis to examine the frequency with which each chromosome is located within a neutrophil lobe with any other (Figure 2A). We find significant non-random distribution of 44 pairs of chromosomes (Table S1). However, this analysis does not consider the character of the chromosomes. For example, a larger chromosome would likely have less lobe partners due simply to occupying more lobe volume. Thus, to avoid the confounding impacts of chromosome character, we repeated our co-localization analysis on randomly shuffled controls (Figure 2B). To generate these shuffled images, we created an imaging framework that randomly places every chromosome (with its individual three-dimensional character and that of the associated nucleus preserved) within the nuclear space of each individual image. Chromosomes were not permitted to overlap one another or the nuclear boundary. This shuffling was performed five independent times for each of the 240 biological images. The colocalization frequency was then examined in each set of shuffled images to determine the variability of shuffling, but more importantly the impact of chromosome character on lobe sharing frequency. The analysis revealed significant lobe sharing in the randomly shuffled images, suggesting that chromosome character does impact lobe distribution.

To overcome the influence of chromosome character on lobe distribution, we filtered our significant lobe partner pairs (Table S1) by significance of co-lobe localization greater than that observed in the randomly shuffled analysis. Eleven chromosome pairings surpassed this threshold (Table S2), suggesting that these chromosomes may preferentially co-localize in neutrophil nuclear lobes. However, the pairs in question share very similar spectral combinations, suggesting that perhaps the significance observed is an artifact of miscalling. For example, if one region of chromosome 1 (painted Cy5) was occasionally miscalled as chromosome 6 (painted Cy5 and FITC) or vice versa this could lead to a significant colocalization score.

To validate our chromosome paint findings, we performed an orthogonal analysis of chromosome proximity using *in situ* HiC (Rao et al., 2014). *In situ* HiC utilizes proximity ligation to determine the three-dimensional association of regions of DNA in populations of fixed nuclei (Figure 2C and Supplemental information). While in most cells the vast majority of ligation events occur within chromosomes, transchromosomal interactions can be used as a measure of chromosome-chromosome proximity (Rao et al., 2014). Performing *in situ* HiC on human neutrophils, we find that they exhibit dramatically more transchromosomal interaction than human immune cell types with spherical nuclei (Figure 2D). This is likely due to the increased physical confinement within neutrophil nuclei (Zhu et al., 2017). If, as hinted at by chromosome paint, particular chromosomes are more frequently co-localized to neutrophil nuclear lobes than expected by chance, we would expect to observe an enrichment of transchromosomal interactions between these chromosomes compared to other chromosome pairs. However, we find that the distribution of transchromosomal interactions in human blood neutrophils is predominantly dependent on chromosome length (r^2 = 0.968, Figure 2E) with no notable increase in interaction observed between any of the chromosome pairs suggested to co-localize by chromosome paint (Figure 2F).

Thus, using two independent methods, and by comparing to randomly shuffled controls, we find no consistent evidence of non-random chromosome distribution to human neutrophil nuclear lobes.

Human neutrophil chromosomes do not position randomly within nuclear lobes

Consistent with findings in spherical nuclei (Bolzer et al., 2005), our distribution analysis finds that the proximity pattern of chromosomes within neutrophil nuclei is random. Alongside random proximity pattern, non-random radial chromosome distribution is also well documented. As such, larger chromosomes are consistently observed closer to the nuclear periphery than their more diminutive counterparts (Bolzer et al., 2005). This has even been observed in a handful of neutrophil chromosomes (Hubner et al., 2015).

To determine whether all human neutrophil chromosomes exhibit this relationship with the nuclear periphery, we examined the position of chromosomes relative to the lobed nuclear membrane. To do so, we first break the radius of each lobe into a continuous scale from 0 to 1, 1 being the three-dimensional center of the lobe and 0 being the nuclear periphery (Figure 3A). We then give each chromosome within the lobe a value between 0 and 1 based upon the mean position of its total volume (Figure 3B). By applying this method to all chromosomes in all lobes, we are able to determine the position of each chromosome relative to the lobe boundary. As such, we find a significant relationship between chromosome linear length and its relative position within a lobe ($r^2 = 0.749$, $p = 4.60 \times 10^{-8}$), with larger chromosomes more likely to be found nearer the nuclear periphery than shorter chromosomes (Figure 3C). Importantly, when we apply this same method to our randomly shuffled control images the association is no longer detected (Figure 3D), strongly suggesting that it is not simply the volume of the larger chromosomes underlying the relationship. Similarly, when we examined the relationship between chromosome gene-density (genes/Mb) and radial position, we find gene dense chromosomes trend toward being positioned near the lobe center more than gene-poor chromosomes (Figure S4E), consistent with previous works (Bolzer et al., 2005).

Thus, as in spherical nuclei, chromosomes within the highly physically restricted neutrophil nuclear lobes are positioned in a non-random size- and gene density-influenced manner.

DISCUSSION

Human blood neutrophils have been identified for over a hundred years by their numerous nuclear lobes separated by fantastically thin filaments of nucleoplasm (P Ehrlich, 1900). Unfortunately for studies such as ours, fixation can lead to significant changes to this morphology, particularly the clustering of nuclear lobes. While these fixation-dependent changes can cause problems (Hepperger et al., 2007), here, while it made lobe identification more challenging, the observation of previously reported non-random radial distribution of chromosomes within lobes suggests that fixation did not significantly alter neutrophil chromosome territorial organization.

The similarities in chromosome position between lobed neutrophil nuclei and spherical nuclei suggest that neutrophil chromosomes simply move and adapt to the more restricted nuclear environment created by lamin-mediated constriction (Skinner and Johnson, 2017). Thus, it appears that most chromosomes are simply passengers in the lobing process. However, there is one chromosome that appears to influence nuclear morphology – the inactive X chromosome. As such, the inactive X chromosome is frequently located within a small appendage protruding from the terminal lobe of female neutrophil nuclei (Aquiles Sanchez et al., 1997; Hoffmann et al., 2007; Karni et al., 2001). Strong evidence that the inactive X chromosome influences the formation of these appendages comes from the neutrophils of XXX or XXXX individuals which frequently exhibit two or three appendages, respectively (Aquiles Sanchez et al., 1997). How the inactive X chromosome itself, its epigenetic state or its associated factors drive the formation of the nuclear appendages is unclear. However, these unique appendages do suggest that chromosomes are not always simply passive during nuclear morphology changes, but can under certain circumstances influence the process.

Compared to their precursors and other immune cells, mature neutrophils are transcriptionally muted (Gemelli et al., 2006; Hubner et al., 2015; Newburger et al., 2000). It is unclear why. Prior to our study, one possibility was that neutrophil lobing perturbed the macroscale organization of chromosomes, and thus their transcriptional activity. However, consistent with examinations of fewer (between 4 and 7) chromosomes (Aquiles Sanchez et al., 1997; Hubner et al., 2015), we find that chromosome territories remain highly organized within neutrophil nuclear lobes. Thus, overt chromosomal disorganization does not appear to explain the relative transcriptional inactivity of neutrophils.

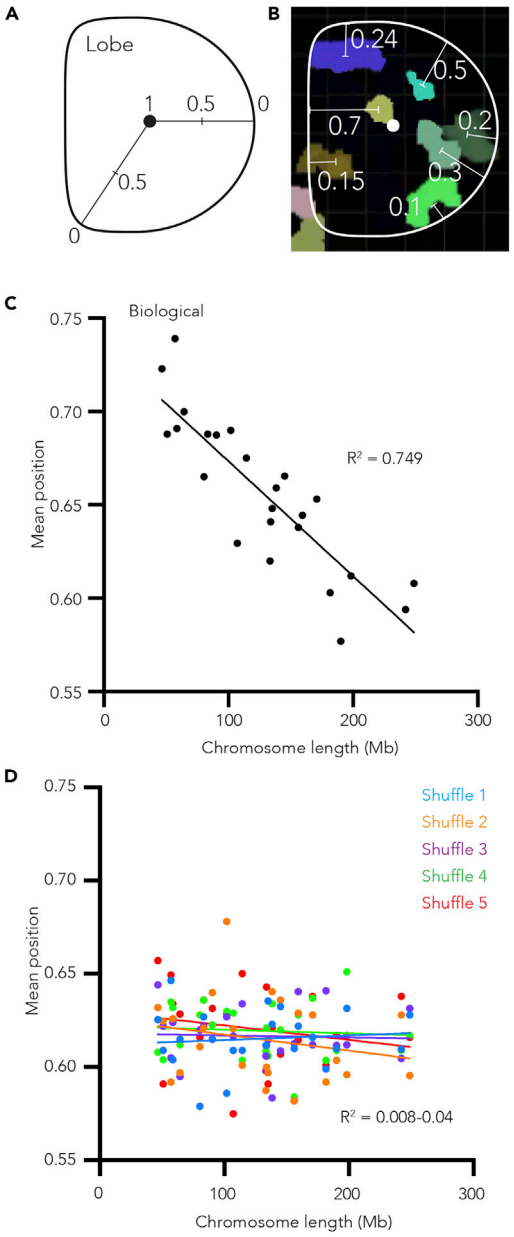

Figure 3. Human neutrophil chromosomes do not position randomly within nuclear lobes

(A) Schematic showing how radial position values within a neutrophil nuclear lobe are calculated.

(B) A slice through a neutrophil nuclear lobe image showing the approximate radial position values of the chromosomes. For clarity most chromosomes are not shown.

(C) Scatterplot of the median of the mean chromosome volume radial position within human neutrophil nuclear lobes plotted as a function of chromosome length (Mb). Straight line fitted to data ($y = -6.18e\text{-}4x+0.735$, $R^2 = 0.7498$ and p value 4.6×10^{-8}).

(D) Scatterplot of the median of the mean chromosome volume radial position from five independent sets of random chromosome position shufflings plotted as a function of chromosome length (Mb). Straight line fitted to each instance independently ($y = -2.38e\text{-}5x+0.612$, $R^2 = 0.008$ and p value = not significant (ns), $y = -8.47e\text{-}5x+0.612$, $R^2 = 0.0473$ and p value ns, $y = -1.24e\text{-}5x+0.618$, $R^2 = 0.0023$ and p value ns, $y = -2.12e\text{-}5x+0.622$, $R^2 = 0.0066$ and p value ns, $y = -7.45e\text{-}5x+0.630$, $R^2 = 0.0378$ and p value ns).

It has been previously reported that regions on one chromosome can influence the expression of a gene on another, presumably via three-dimensional physical proximity (Williams et al., 2010). These interactions are known as gene regulatory transchromosomal interactions (Kioussis, 2005). Interestingly, these interactions have been predominantly reported in immune cells (Hewitt et al., 2008; Johanson et al., 2019; Kim et al., 2014; Ling et al., 2006; Spilianakis et al., 2005; Zhao et al., 2006). However, both their function and indeed existence is debated (Johanson et al., 2018). Here, while we reveal relatively large numbers of transchromosomal interactions in neutrophil nuclei via *in situ* HiC, our data suggest little to no preferential distribution of chromosomes to neutrophil nuclear lobes (where chromosomes are physically constrained and could physically interact only with their lobe mates), which suggests that gene regulatory transchromosomal interactions are unlikely to occur in mature human neutrophils.

The non-random radial distribution of chromosomes we have detected in neutrophil nuclear lobes is common in other cell types (Bolzer et al., 2005) and species (Tanabe et al., 2002). However, the cause and possible purpose of this organization is not known. It has been proposed that the organization could be due to the differential timing of centromere separation (Gerlich et al., 2003) or chromosome position during mitosis (Bolzer et al., 2005), differential interaction between chromosomes and the nuclear periphery and/or other nuclear bodies (Cremer and Cremer, 2001) or simply the force of transcription from highly transcribed chromosomes acting on those lowly transcribed (Yin et al., 1995). A number of purposes for the radial organization have also been proposed, from protecting the genome from viruses and mutagens using a layer of highly repetitive and heterochromatic DNA (Hsu, 1975) to providing nuclear stability or rigidity (Bolzer et al., 2005; Nava et al., 2020; Keenan et al., 2020). Given our findings in the highly malleable neutrophil nuclei the latter seems unlikely. While the function of peripheral heterochromatin is unclear in neutrophils or other cell types, there is one cell type in which the radial position of heterochromatin has a clear function. As the retinal cells of nocturnal animals develop, they invert the vast majority of their heterochromatin from its peripheral position to a central core (Solovei et al., 2009). This remarkable transformation endows the mature retinal cell enhanced light channeling characteristics thus enhancing low light vision.

While many questions remain, here, by leveraging the power provided by our vast data set, we resolve a number of long-standing questions in the field of chromosome organization. We demonstrate in numerous immune cell types that chromosome length has a linear relationship with chromosome volume. Moreover, in human neutrophils we show that chromosome lobe distribution is random, while chromosome radial position within lobes is non-random, expanding our knowledge of this remarkably abundant, but poorly understood immune cell.

Limitations of the study

As shown and discussed above, fixation of the human blood neutrophil nuclei leads to changes in their lobed morphology. While this does not appear to prohibit meaningful insight, it should be considered when interpreting the results presented.

Resource availability

Lead contact

Further information and requests for resources and data should be directed to the lead contact, Timothy Johanson (johanson@wehi.edu.au), The Walter and Eliza Hall Institute of Medical Research, Parkville, VIC, 3052, Australia.

Materials availability

This study did not generate new unique reagents.

Data and code availability

Sequence data that support the findings of this study are tabulated in the supplementary tables and are available in the GEO database under accession number GSE157229.

METHODS

All methods can be found in the accompanying Transparent Methods supplemental file.

SUPPLEMENTAL INFORMATION

Supplemental information can be found online at https://doi.org/10.1016/j.isci.2021.102161.

ACKNOWLEDGMENTS

The authors thank S. Johanson for constructive discussions, and the volunteers at the Walter and Eliza Hall Volunteer Blood Donor Registry. This work was supported by grants and fellowships from the National Health and Medical Research Council of Australia (T.M.J. #1124081, R.S.A. and T.M.J. #1049307, #1100451, G.K.S. #1058892, R.S.A. and G.K.S. #1158531, C.R.K. #1125436, D.J.H #1113577, L.C.H. #1080887 and #1037321). H.D.C. was supported by an H.C. Marian and E.H. Flack Fellowship. This study was made possible through Victorian State Government Operational Infrastructure Support and Australian Government NHMRC Independent Research Institute Infrastructure Support scheme. The funders had no role in study design, data collection and analysis, decision to publish, or preparation of the manuscript.

AUTHOR CONTRIBUTIONS

C.R.K, M.J.M, N.G.B, G.N, E.C.L, Q.W, C.A.d.G., and T.M.J. designed and conducted experiments; H.D.C. and G.K.S. designed and performed computational analyses; M.J.M., K.L.R., and T.B. designed and executed image analyses; D.J.H., L.C.H., R.S.A., and T.M.J. conceived the study and wrote the manuscript.

DECLARATION OF INTERESTS

The authors declare no competing interests.

Received: October 12, 2020
Revised: November 24, 2020
Accepted: February 3, 2021
Published: March 19, 2021

REFERENCES

Agmon, N., Liefshitz, B., Zimmer, C., Fabre, E., and Kupiec, M. (2013). Effect of nuclear architecture on the efficiency of double-strand break repair. Nat. Cell Biol. *15*, 694–699.

Aquiles Sanchez, J., Karni, R.J., and Wangh, L.J. (1997). Fluorescent in situ hybridization (FISH) analysis of the relationship between chromosome location and nuclear morphology in human neutrophils. Chromosoma *106*, 168–177.

Bartova, E., Kozubek, S., Jirsova, P., Kozubek, M., Lukasova, E., Skalnikova, M., Cafourkova, A., Koutna, I., and Pasekova, R. (2001). Higher-order chromatin structure of human granulocytes. Chromosoma *110*, 360–370.

Bolzer, A., Kreth, G., Solovei, I., Koehler, D., Saracoglu, K., Fauth, C., Muller, S., Eils, R., Cremer, C., Speicher, M.R., and Cremer, T. (2005). Three-dimensional maps of all chromosomes in human male fibroblast nuclei and prometaphase rosettes. PLoS Biol. *3*, e157.

Brianna Caddle, L., Grant, J.L., Szatkiewicz, J., Van Hase, J., Shirley, B.J., Bewersdorf, J., Cremer, C., Arneodo, A., Khalil, A., and Mills, K.D. (2007). Chromosome neighborhood composition determines translocation outcomes after exposure to high-dose radiation in primary cells. Chromosome Res. *15*, 1061–1073.

Cremer, T., and Cremer, C. (2001). Chromosome territories, nuclear architecture and gene regulation in mammalian cells. Nat. Rev. Genet. *2*, 292–301.

Cremer, T., and Cremer, M. (2010). Chromosome territories. Cold Spring Harb. Perspect. Biol. *2*, a003889.

Gemelli, C., Montanari, M., Tenedini, E., Zanocco Marani, T., Vignudelli, T., Siena, M., Zini, R., Salati, S., Tagliafico, E., Manfredini, R., et al. (2006). Virally mediated MafB transduction induces the monocyte commitment of human CD34+ hematopoietic stem/progenitor cells. Cell Death Differ. *13*, 1686–1696.

Gerlich, D., Beaudouin, J., Kalbfuss, B., Daigle, N., Eils, R., and Ellenberg, J. (2003). Global chromosome positions are transmitted through mitosis in mammalian cells. Cell *112*, 751–764.

Hepperger, C., Mayer, A., Merz, J., Vanderwall, D.K., and Dietzel, S. (2009). Parental genomes mix in mule and human cell nuclei. Chromosoma *118*, 335–347.

Hepperger, C., Otten, S., Von Hase, J., and Dietzel, S. (2007). Preservation of large-scale chromatin structure in FISH experiments. Chromosoma *116*, 117–133.

Hewitt, S.L., Farmer, D., Marszalek, K., Cadera, E., Liang, H.E., Xu, Y., Schlissel, M.S., and Skok, J.A. (2008). Association between the Igk and Igh immunoglobulin loci mediated by the 3′ Igk enhancer induces 'decontraction' of the Igh locus in pre-B cells. Nat. Immunol. *9*, 396–404.

Hoffmann, K., Sperling, K., Olins, A.L., and Olins, D.E. (2007). The granulocyte nucleus and lamin B receptor: avoiding the ovoid. Chromosoma *116*, 227–235.

Hsu, T.C. (1975). A possible function of constitutive heterochromatin: the bodyguard hypothesis. Genetics *79*, 137–150.

Hubner, B., Lomiento, M., Mammoli, F., Illner, D., Markaki, Y., Ferrari, S., Cremer, M., and Cremer, T. (2015). Remodeling of nuclear landscapes during human myelopoietic cell differentiation maintains co-aligned active and inactive nuclear compartments. Epigenetics Chromatin *8*, 47.

Johanson, T.M., Chan, W.F., Keenan, C.R., and Allan, R.S. (2019). Genome organization in immune cells: unique challenges. Nat. Rev. Immunol. *19*, 448–456.

Johanson, T.M., Coughlan, H.D., Lun, A.T.L., Bediaga, N.G., Naselli, G., Garnham, A.L., Harrison, L.C., Smyth, G.K., and Allan, R.S. (2018). Genome-wide analysis reveals no evidence of trans chromosomal regulation of mammalian immune development. PLoS Genet. *14*, e1007431.

Karni, R.J., Wangh, L.J., and Sanchez, J.A. (2001). Nonrandom location and orientation of the inactive X chromosome in human neutrophil nuclei. Chromosoma *110*, 267–274.

Keenan, C.R., Coughlan, H.D., Iannarella, N., Johanson, T.M., Chan, W.F., Garnham, A.L., Smyth, G.K., and Allan, R.S. (2020). Suv39h-catalysed H3K9me3 is critical for euchromatic genome organisation and the maintenance of gene transcription. bioRxiv.

Khalil, A., Grant, J.L., Caddle, L.B., Atzema, E., Mills, K.D., and Arneodo, A. (2007). Chromosome

territories have a highly nonspherical morphology and nonrandom positioning. Chromosome Res. *15*, 899–916.

Kim, L.K., Esplugues, E., Zorca, C.E., Parisi, F., Kluger, Y., Kim, T.H., Galjart, N.J., and Flavell, R.A. (2014). Oct-1 regulates IL-17 expression by directing interchromosomal associations in conjunction with CTCF in T cells. Mol. Cell *54*, 56–66.

Kioussis, D. (2005). Gene regulation: kissing chromosomes. Nature *435*, 579–580.

Ling, J.Q., Li, T., Hu, J.F., Vu, T.H., Chen, H.L., Qiu, X.W., Cherry, A.M., and Hoffman, A.R. (2006). CTCF mediates interchromosomal colocalization between Igf2/H19 and Wsb1/Nf1. Science *312*, 269–272.

Nava, M.M., Miroshnikova, Y.A., Biggs, L.C., Whitefield, D.B., Metge, F., Boucas, J., Vihinen, H., Jokitalo, E., Li, X., Garcia Arcos, J.M., et al. (2020). Heterochromatin-driven nuclear softening protects the genome against mechanical stress-induced damage. Cell *181*, 800–817 e22.

Newburger, P.E., Subrahmanyam, Y.V., and Weissman, S.M. (2000). Global analysis of neutrophil gene expression. Curr. Opin. Hematol. *7*, 16–20.

P Ehrlich, A.L. (1900). Die Anæmie, Nothnagel's Specielle Pathologie und Therapie, Alfred Höder, Wien u. Leipzig.

Parada, L.A., Mcqueen, P.G., and Misteli, T. (2004). Tissue-specific spatial organization of genomes. Genome Biol. *5*, R44.

Parada, L.A., Mcqueen, P.G., Munson, P.J., and Misteli, T. (2002). Conservation of relative chromosome positioning in normal and cancer cells. Curr. Biol. *12*, 1692–1697.

Rabl, C. (1885). Uber zelltheilung. Morphol. Jahrb. *10*, 214–330.

Rao, S.S., Huntley, M.H., Durand, N.C., Stamenova, E.K., Bochkov, I.D., Robinson, J.T., Sanborn, A.L., Machol, I., Omer, A.D., Lander, E.S., and Aiden, E.L. (2014). A 3D map of the human genome at kilobase resolution reveals principles of chromatin looping. Cell *159*, 1665–1680.

Roix, J.J., Mcqueen, P.G., Munson, P.J., Parada, L.A., and Misteli, T. (2003). Spatial proximity of translocation-prone gene loci in human lymphomas. Nat. Genet. *34*, 287–291.

Skinner, B.M., and Johnson, E.E. (2017). Nuclear morphologies: their diversity and functional relevance. Chromosoma *126*, 195–212.

Solovei, I., Kreysing, M., Lanctot, C., Kosem, S., Peichl, L., Cremer, T., Guck, J., and Joffe, B. (2009). Nuclear architecture of rod photoreceptor cells adapts to vision in mammalian evolution. Cell *137*, 356–368.

Spilianakis, C.G., Lalioti, M.D., Town, T., Lee, G.R., and Flavell, R.A. (2005). Interchromosomal associations between alternatively expressed loci. Nature *435*, 637–645.

Tanabe, H., Muller, S., Neusser, M., Von Hase, J., Calcagno, E., Cremer, M., Solovei, I., Cremer, C., and Cremer, T. (2002). Evolutionary conservation of chromosome territory arrangements in cell nuclei from higher primates. Proc. Natl. Acad. Sci. U S A *99*, 4424–4429.

Williams, A., Spilianakis, C.G., and Flavell, R.A. (2010). Interchromosomal association and gene regulation in trans. Trends Genet. *26*, 188–197.

Yerle-Bouissou, M., Mompart, F., Iannuccelli, E., Robelin, D., Jauneau, A., Lahbib-Mansais, Y., Delcros, C., Oswald, I.P., and Gellin, J. (2009). Nuclear architecture of resting and LPS-stimulated porcine neutrophils by 3D FISH. Chromosome Res. *17*, 847–862.

Yin, H., Wang, M.D., Svoboda, K., Landick, R., Block, S.M., and Gelles, J. (1995). Transcription against an applied force. Science *270*, 1653–1657.

Zhao, Z., Tavoosidana, G., Sjolinder, M., Gondor, A., Mariano, P., Wang, S., Kanduri, C., Lezcano, M., Sandhu, K.S., Singh, U., et al. (2006). Circular chromosome conformation capture (4C) uncovers extensive networks of epigenetically regulated intra- and interchromosomal interactions. Nat. Genet. *38*, 1341–1347.

Zhu, Y., Gong, K., Denholtz, M., Chandra, V., Kamps, M.P., Alber, F., and Murre, C. (2017). Comprehensive characterization of neutrophil genome topology. Genes Dev. *31*, 141–153.

iScience, Volume *24*

Supplemental information

Chromosomes distribute randomly to, but not within, human neutrophil nuclear lobes

Christine R. Keenan, Michael J. Mlodzianoski, Hannah D. Coughlan, Naiara G. Bediaga, Gaetano Naselli, Erin C. Lucas, Qike Wang, Carolyn A. de Graaf, Douglas J. Hilton, Leonard C. Harrison, Gordon K. Smyth, Kelly L. Rogers, Thomas Boudier, Rhys S. Allan, and Timothy M. Johanson

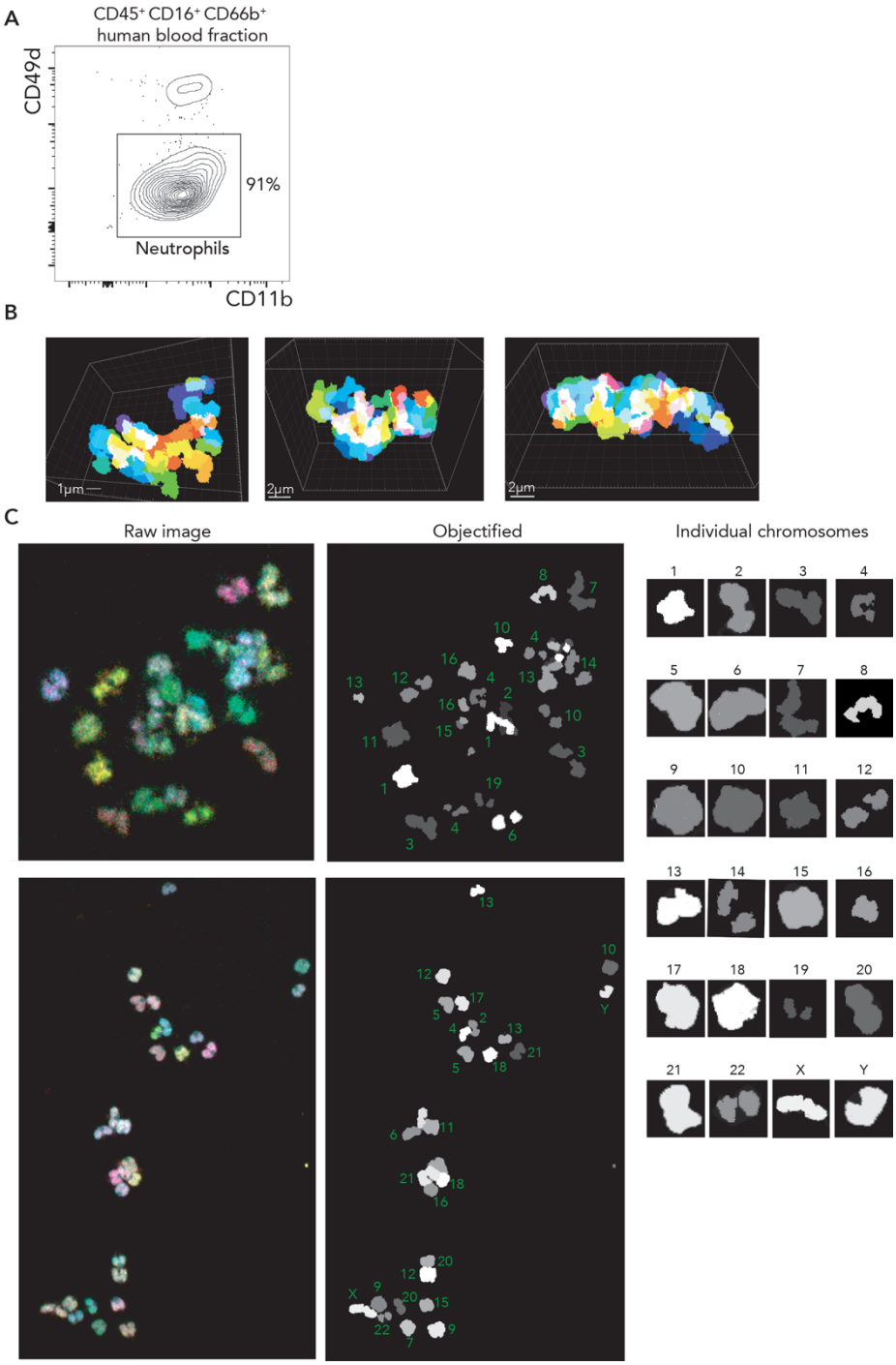

Supp Fig 1. Neutrophil isolation and chromosome paint quality control. Related to Fig 1. (A) Example purity check of enriched human blood neutrophils. (B) Example 3D renders of human neutrophil nuclei. Colours are arbitrary but represent individual chromosomes. (C) Example of chromosome calling using our analysis pipeline on human metaphase chromosome spreads. Raw images (left), objectified images (centre) with called chromosome number, and select individual chromosomes (right) are shown.

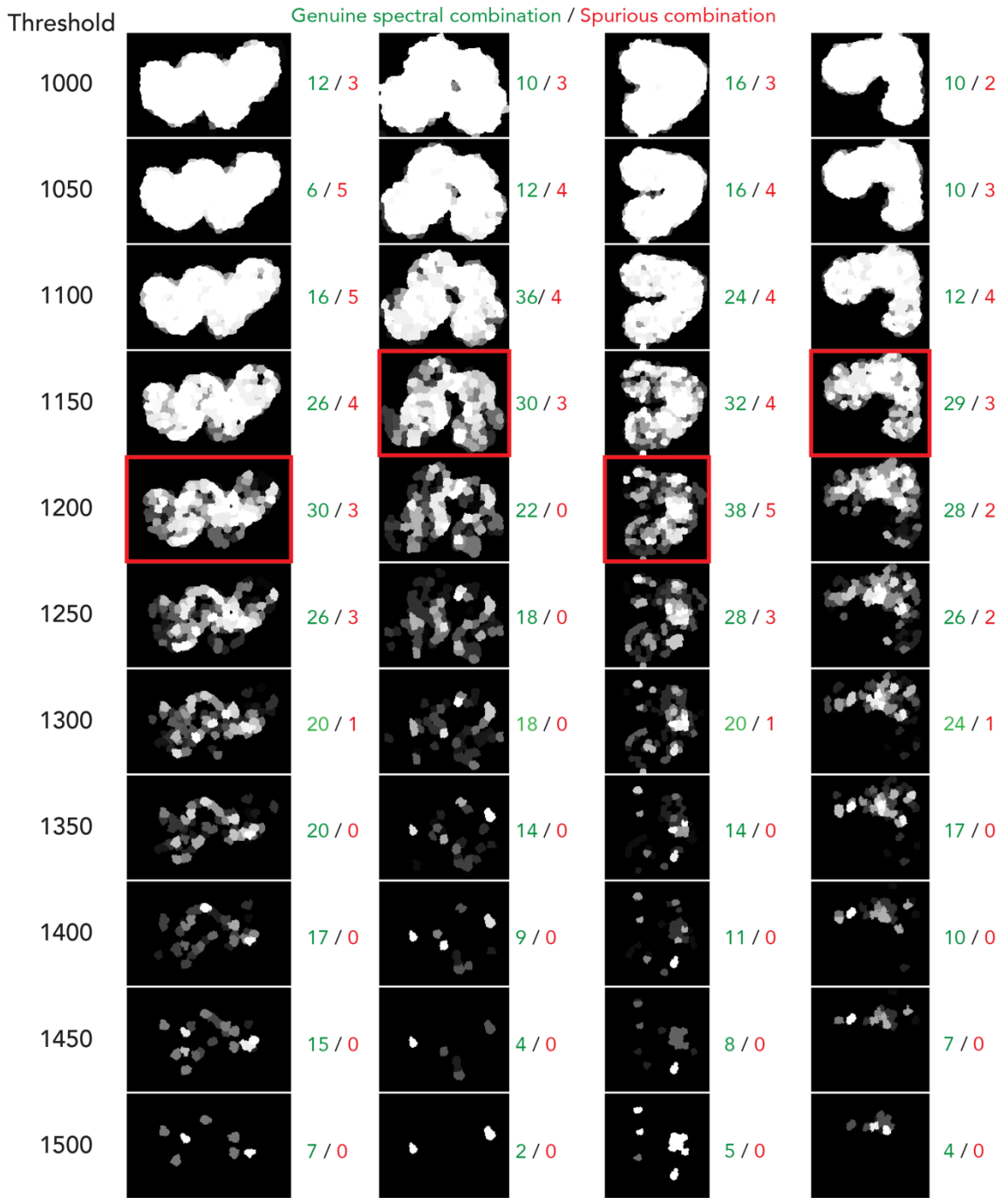

Supp Fig 2 Serial thresholding. Related to Fig 1. Images showing the number of objects called with genuine spectral combinations (green) and spurious combinations (red) in four select neutrophil nuclei images at thresholds between 1000 and 1500. Red boxed image shows the threshold closest to that called by the algorithm. For clarity, examples of images thresholded in increments of 50 are shown. In fact, increments of 10 are used by the algorithm.

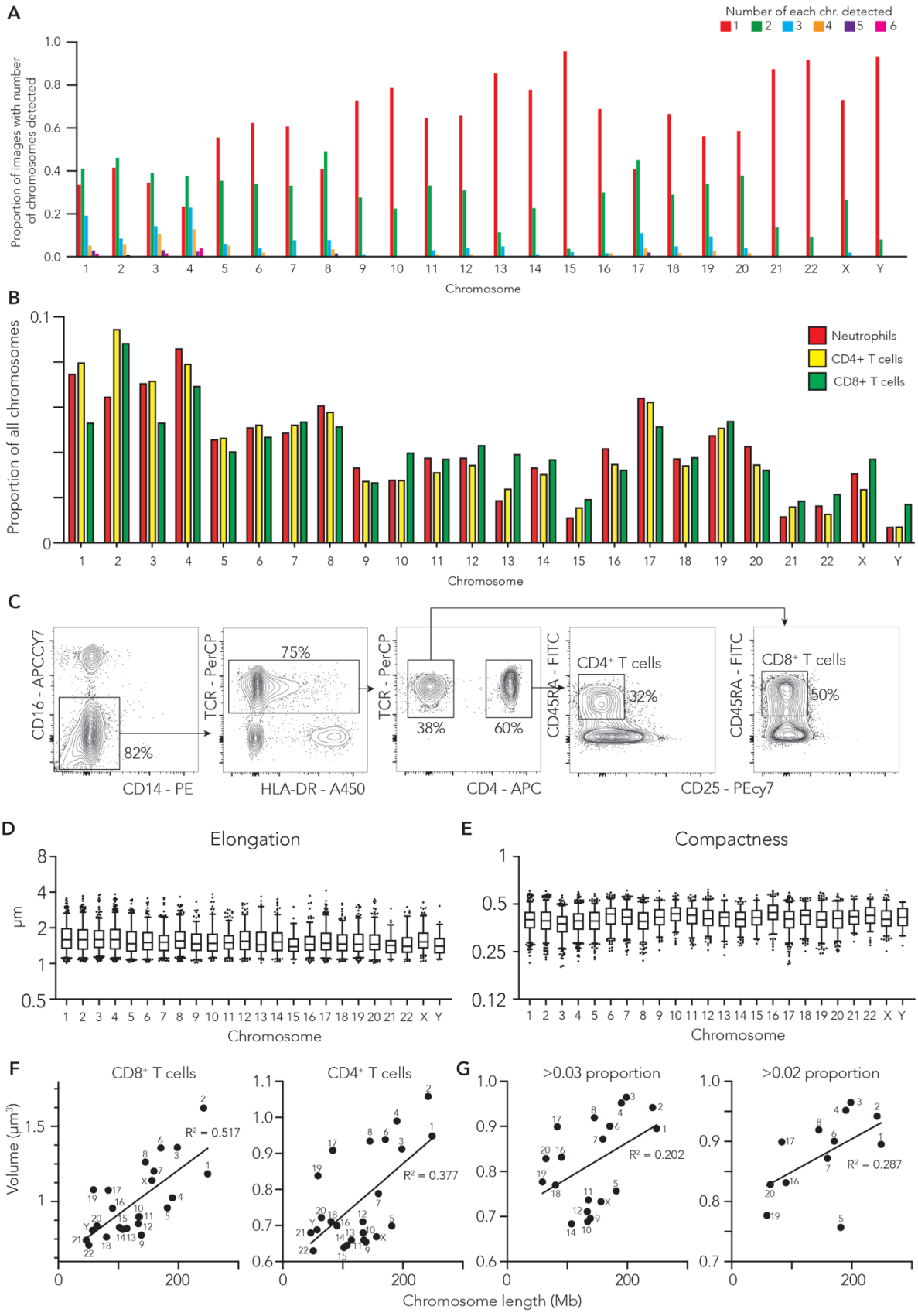

Supp Fig 3 Detecting and measuring chromosomes. Related to Fig 1. (A) Number of chromosomes defined within a nucleus for all neutrophil images (proportion shown). (B) Proportion

of total chromosomes detected made up by each chromosome in human blood neutrophils, $CD4^+$ T cells and $CD8^+$ T cells. Data from 171 $CD4^+$ T cells and 30 $CD8^+$ T cells. (C) Example sort profile of human blood CD4+ and CD8+ T cells. (D, E) Box and whisker plot (5^{th}-95^{th} percentile) showing the elongation (D) and compactness (E) of chromosomes detected in human blood neutrophils. Elongation is the ratio between the largest axis of a fitted 3D ellipsoid and the second largest. Compactness is the normalized ratio between volume and surface. (F) Scatterplot of median chromosome volume in $CD8^+$ T cells (left) and $CD4^+$ T cells (right) against chromosome linear length. Data fitted with a straight line (y=2.94e-3x+0.621, $R^2 = 0.517$ and p-value 7.5e-5 and y=1.41e-3x+0.588, $R^2 = 0.377$ and p-value 0.00141, respectively). (G) Scatterplot of median chromosome volume in neutrophils excluding chromosomes called at a proportion of total lower than 0.03 (left) and 0.02 (right) against chromosome linear length. Data fitted with a straight line (y=7.93e-4x+0.704, $R^2 = 0.202$ and p-value 0.0753 and y=5.48e-3x+0.794, $R^2 = 0.287$ and p-value 0.072, respectively).

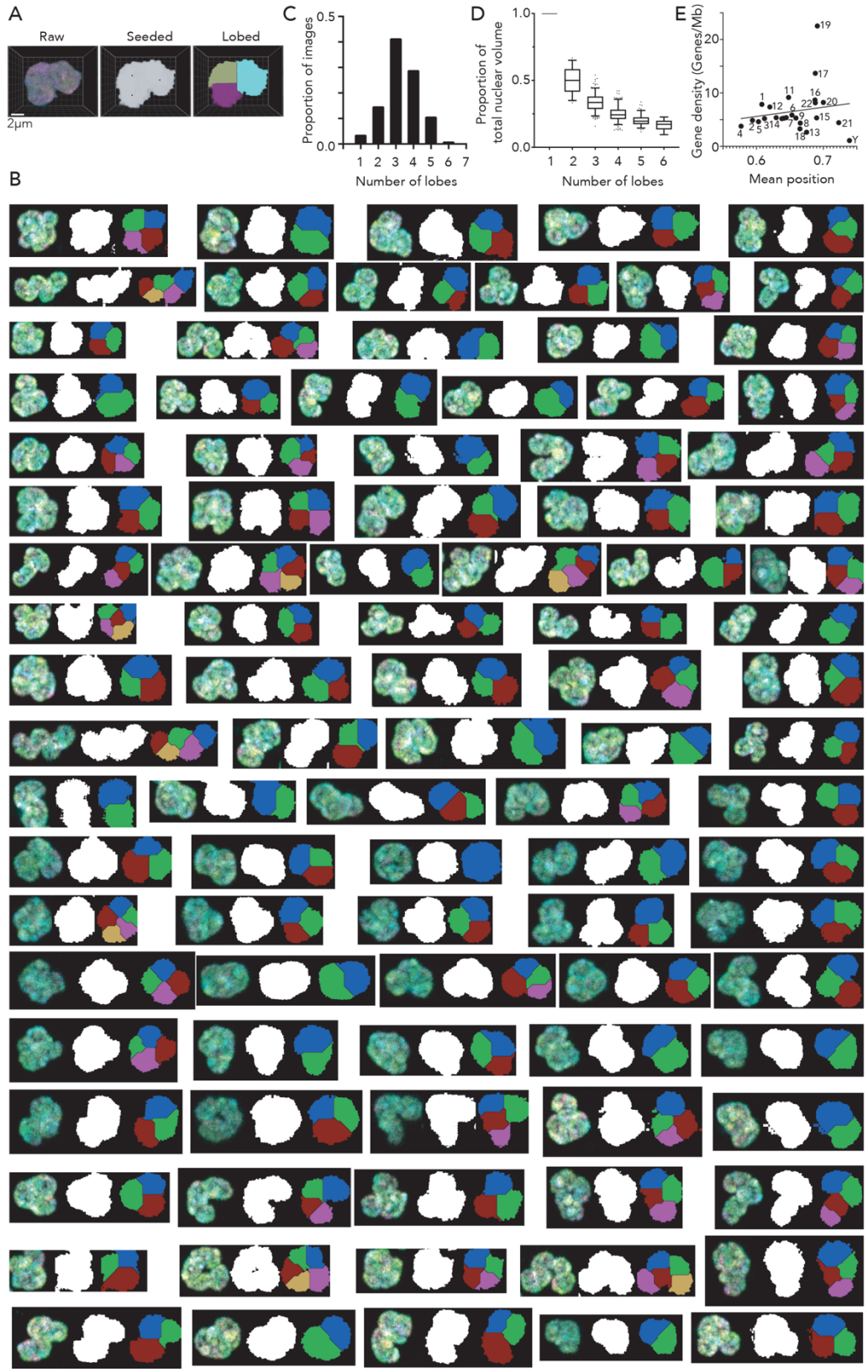

Supp Fig 4 Defining nuclear lobes. Related to Fig 2. (A) Slice of a neutrophil image moving through the lobe calling pipeline, from raw image to the final lobed nucleus defined using watershed analysis. (B) Further examples of lobe calling pipeline results. (C) Bar plot showing the proportion of

human blood neutrophils containing between 1-7 nuclear lobes. (D) Box and whisker plot (5^{th}-95^{th} percentile) showing the volume of lobes as a proportion of the total nuclear volume in human blood neutrophils containing between 1-6 lobes. (E) Scatterplot of the median of the mean chromosome volume radial position within human neutrophil nuclear lobes plotted as a function of gene density (genes/Mb). Data fitted with a straight line (y=17.29e-4x-4.77, $R^2 = 0.028$ and p-value 0.433).

Transparent Methods

Ethics Statement

Collection of human blood for research studies was approved by Human Research Ethics Committees of Melbourne Health and Walter and Eliza Hall Institute of Medical Research (application 88/03). Written consent was obtained from donors. Donors were all males aged between 25-40 years of age.

Cell isolation

Neutrophils were isolated from 2ml of healthy male donor whole blood following the EasySep Human Neutrophil Enrichment kit manufacturer's protocol). Purity was ~90%. Human T cells were isolated from the PBMC layer of the remaining whole blood after density separation in Leucosep™ tubes containing 15 mL Ficoll-Paque, following the manufacturer's protocol. These cells were stained with TCRab-PerCP-eFluor 710 (eBioscience Cat.No. 46-9986-42), CD4-APC (BD Pharmingen Cat.No. 555349), CD25-PECy7 (BD Bioscience Cat.No. 557741), CD45RA-FITC (eBioscience Cat.No. 556626), CD14-PE (BioLegend Cat.No. 367104), CD16- APC-Cy7 (BD Bioscience Cat.No. 557758), HLA-DR-eFluor450 (eBioscience Cat.No. 48-9952-42) and CD19-BV650 (BioLegend Cat.No. 302238). CD4+ T cells (CD16- CD14- TCRab+ CD4+ CD45RA+ CD25-) and CD8+ T cells (CD16- CD14- TCRab+ CD4- CD45RA+ CD25-) were sorted to a purity >97%.

Chromosome paint

Sixty thousand cells were settled on a poly-L-Lysine (Sigma Aldrich Cat no. P4707) coated cover slip at 37^{o}C for 20 minutes, washed with phosphate buffer saline, before fixing with fresh 3:1 methanol:acetic acid (glacial) for 15 minutes at 22^{o}C. The cells were then rinsed twice with water before being incubated in 2x saline-sodium citrate buffer (SSC) for 2 minutes. The cells were then dehydrated in an ethanol series (75%, 85% and 100%) for 2 minutes each. 7uL of Metasystems

24XCyte Human multicolour FISH probes (Metasystems Cat no. D-0125-060-DI) was pre-warmed on a glass slide at 37°C for 5 minutes before a further 2 minutes at 75°C with the cells added. The cells were then sealed and incubated at 37°C for 18 hours in a dark, humid chamber. After hybridisation was complete the cells were immersed in 72°C 0.4x SSC for 2 minutes, 2x SSC with 0.05% Tween-20 for 30 seconds before being sealed on a glass slide in 85% glycerol.

Confocal Microscopy

Imaging experiments were performed on a Zeiss 880 confocal microscope using a 63x 1.4 NA objective lens. The system was run in lambda mode, recording fluorescence signal in 32 spectral channels over a spectral range of 410 nm to 690 nm (in 8.9 nm increments). Samples were imaged in 3D using Nyquist sampling of 70 nm pixel size and z-steps of 200 nm using the 405 nm, 488 nm, 561 nm and 633 nm lasers to excite the samples consisting of the fluorescent labels DEAC, FITC, Spectrum Orange, Texas Red and Cy5. Single colour control experiments were performed to determine the spectral signatures using the above microscope settings.

Tetraspeck beads (ThermoFisher) adhered to a coverslip and mounted to a microscope slide were imaged in 3D. Custom written Matlab (Mathworks, Natick, MA, USA) scripts measured the axial positions of the Tetraspeck beads in each spectral channel and removed the chromatic aberrations from the sample images. The five spectral signatures from the single colour controls were used to linearly unmix the 32-channel spectral fluorescence signal in each voxel into the five constituent fluorophores.

Chromosome assignment and measurement

After channel unmixing and normalisation, voxels with similar values in the 5 channels are clustered together using a 3D Simple Linear Iterative Clustering (SLIC) algorithm (Tran Thi Nhu et al., 2017). Thresholding is then applied to the 5 channels and chromosome identity is assigned according to known channel combinations. The threshold is set automatically by examining a range of thresholds

and select that which yields the optimal number of chromosome objects (2) and the minimum number of false combination objects. Chromosome measurements are performed on assigned chromosomes using algorithms and tools from the 3D ImageJ suite (Ollion et al., 2013). 3D Eroded Volume Fraction (Ballester et al., 2008) is also performed to compute the position of chromosomes within the nucleus.

Nuclear lobe calling

Nuclei boundaries are detected by summing all channels and global thresholding. The approximate 3D positions of the lobe centres are manually marked before a watershed method separates the nucleus into lobes.

Chromosome shuffling

While considering the chromosomes three-dimensional character, the centre positions of all chromosomes are randomly distributed within the nuclear space until all chromosomes fit and no overlapping is observed between chromosomes. Due to space constraints shuffling was not possible for every nucleus attempted.

All images were stored within an OMERO Database (Allan et al., 2012), processing and analysis were then automated using the TAPAS home system (Whitehead, 2018).

Chromosome measurements analysis

Chromosome measurements were analysed with R using packages dplyr and purr. Objects not assigned to a known combination of values were removed for analysis and plotting. Straight lines were fitted to the data with function lm() from R.

Chromosome co-localisation in lobes

Nuclei with less than ten chromosomes detected or just one lobe were excluded from the analysis. For the remaining nuclei, the volume of each chromosome in each lobe was recorded. The co-localisation

score of any two chromosomes in a nucleus was quantified by $Sum(p_{il} * p_{jl})$, where p_{il} is the proportion by volume of chromosome i in lobe l , p_{jl} is the proportion by volume of chromosome j in lobe l , and the sum is over all lobes in the nucleus. Co-localization p-values were obtained as follows. Each chromosome was treated in turn as the reference chromosome. The co-localisation scores for the reference chromosome with each other chromosome were ranked within each nucleus. The ranks were summed across nuclei and converted to z-scores assuming uniformly distributed ranks for each nucleus. The p-values were adjusted for multiple testing using the Bonferroni correction. Heatmaps of the $-\log_{10}$(p-value) were generated using the R package gplots with the function heatmap.2.

***In situ* HiC**

As described by Rao et al. (Rao et al., 2014), $2x10^6$ human blood neutrophils were resuspended with culture media at $1x10^6$ cells/ml and fixed with 1% v/v formaldehyde (Sigma). Crosslinked cells were lysed with 10mM Tris-HCl pH8.0, 10 mM NaCl, 0.2% Igepal CA630 (Sigma), and protease inhibitors (Sigma). Pelleted nuclei were then digested with 100U of MboI (NEB) overnight and subsequently biotin-labelled with Klenow fragment (NEB) and biotin-dATP (Invitrogen). Filled ends were ligated with T4 DNA ligase (NEB) and sonicated (Covaris). The resulting DNA fragments were biotin-pulled down and end-repaired with T4 polynucleotide kinase (NEB), T4 DNA polymerase (NEB) and Klenow fragment, followed by A-tailing with 3'-5' Klenow (exo-) fragment (NEB), and adaptor ligation using Quick ligase (NEB). The resultant Hi-C library was amplified with Phusion Polymerase (Thermo), size-selected and purified with AMPure XP magnetic beads (Beckman) and sequenced on an Illumina NextSeq 500 to produce 81-bp paired-end reads. Approximately 200 million read pairs were generated for one biological replicate.. HiC libraries for $CD4^+$ T cells, $CD8^+$ T cells and B cells are from GSE105776. The data pre-processing and analysis was performed with the *diffHic* pipeline (Lun and Smyth, 2015) in R with changes in parameters (Johanson et al., 2018a). Where biological replicates were available, the libraries were summed after pre-processing.

Chromosomal looping interactions were detected using a method described by Rao et al. (Rao et al., 2014) and in (Johanson et al., 2018b). In brief, read pairs were counted in bin pairs of 50 kbp anchors for all libraries. For each bin pair, the log-fold change over the average abundance of each of several neighbouring regions was computed. Neighbouring regions in the interaction space included a square quadrant of sides 'x+1' that was closest to the diagonal and contained the target bin pair in its corner; a horizontal stripe of length '2x+1' centred on the target bin pair; a vertical stripe of '2x+1', similarly centred; and a square of sides '2x+1', also containing the target bin pair in the centre. The enrichment value for each bin pair was defined as the minimum of these log-fold changes, i.e., the bin pair had to have intensities higher than all neighbouring regions to obtain a large enrichment value. The neighbourhood counts for the libraries at 50 kbp bin size were computed with the neighborCounts function from the *diffHic* package with flank (x) 5 bin sizes (i.e., 250 kbp) and enrichment values were determined with filterPeaks function with get.enrich=TRUE. Looping interactions were then filtered with filterPeaks. Loops were defined as those with enrichment values above 1, were more than 100 kbp from the diagonal and with minimum count greater than 10 for all libraries except the neutrophils which used a minimum count of 5 to accounts for differences in library size. Directly adjacent loops in the interaction space were aggregated into clusters to a maximum cluster size of 500 kbp using the clusterPairs function from the *csaw* package v1.18.0 (Lun and Smyth, 2016). Blacklisted genomic regions were obtained from ENCODE for hg38 (Consortium, 2012). Loops that that had at least one anchor in a blacklisted genomic region were removed.

Heatmaps of the loops between chromosomes where generated using the R package gplots with the function heatmap.2. The frequency of transchromosomal interactions to the power of 0.25 was plotted as a function of the sum of the chromosome lengths. A linear model was fitted to data with the lm function.

Supplemental References

ALLAN, C., BUREL, J. M., MOORE, J., BLACKBURN, C., LINKERT, M., LOYNTON, S., MACDONALD, D., MOORE, W. J., NEVES, C., PATTERSON, A., PORTER, M., TARKOWSKA, A., LORANGER, B., AVONDO, J., LAGERSTEDT, I.,

LIANAS, L., LEO, S., HANDS, K., HAY, R. T., PATWARDHAN, A., BEST, C., KLEYWEGT, G. J., ZANETTI, G. & SWEDLOW, J. R. 2012. OMERO: flexible, model-driven data management for experimental biology. *Nat Methods,* 9**,** 245-53.

BALLESTER, M., KRESS, C., HUE-BEAUVAIS, C., KIEU, K., LEHMANN, G., ADENOT, P. & DEVINOY, E. 2008. The nuclear localization of WAP and CSN genes is modified by lactogenic hormones in HC11 cells. *J Cell Biochem,* 105**,** 262-70.

CONSORTIUM, E. P. 2012. An integrated encyclopedia of DNA elements in the human genome. *Nature,* 489**,** 57-74.

JOHANSON, T. M., COUGHLAN, H. D., LUN, A. T. L., BEDIAGA, N. G., NASELLI, G., GARNHAM, A. L., HARRISON, L. C., SMYTH, G. K. & ALLAN, R. S. 2018a. Genome-wide analysis reveals no evidence of trans chromosomal regulation of mammalian immune development. *PLoS Genet,* 14**,** e1007431.

JOHANSON, T. M., LUN, A. T. L., COUGHLAN, H. D., TAN, T., SMYTH, G. K., NUTT, S. L. & ALLAN, R. S. 2018b. Transcription-factor-mediated supervision of global genome architecture maintains B cell identity. *Nat Immunol,* 19**,** 1257-1264.

LUN, A. T. & SMYTH, G. K. 2015. diffHic: a Bioconductor package to detect differential genomic interactions in Hi-C data. *BMC Bioinformatics,* 16**,** 258.

LUN, A. T. & SMYTH, G. K. 2016. csaw: a Bioconductor package for differential binding analysis of ChIP-seq data using sliding windows. *Nucleic Acids Res,* 44**,** e45.

OLLION, J., COCHENNEC, J., LOLL, F., ESCUDE, C. & BOUDIER, T. 2013. TANGO: a generic tool for high-throughput 3D image analysis for studying nuclear organization. *Bioinformatics,* 29**,** 1840-1.

RAO, S. S., HUNTLEY, M. H., DURAND, N. C., STAMENOVA, E. K., BOCHKOV, I. D., ROBINSON, J. T., SANBORN, A. L., MACHOL, I., OMER, A. D., LANDER, E. S. & AIDEN, E. L. 2014. A 3D map of the human genome at kilobase resolution reveals principles of chromatin looping. *Cell,* 159**,** 1665-80.

TRAN THI NHU, H., ARROJO, E. D. R., BERGGREN, P. O. & BOUDIER, T. 2017. A novel toolbox to investigate tissue spatial organization applied to the study of the islets of Langerhans. *Sci Rep,* 7**,** 44261.

WHITEHEAD, L., WIMMER, V., LAFOURESSE, F., RATNAYAKE, D., CURRIE, P., GROOM, J., ROGERS, K. AND BOUDIER, T 2018. Towards an Automated Processing and Analysis System for multi-dimensional light-sheet microscopy big data using ImageJ and OMERO. *International Microscopy Congress IMC 19.*